Recent progress in the research of inorganic fullerene-like nanoparticles and inorganic nanotubes

Reshef Tenne*[a] and Meir Redlich[b]

Received 26th August 2009
First published as an Advance Article on the web 3rd December 2009
DOI: 10.1039/b901466g

Nanoparticles of inorganic compounds with layered (2D) structures, like graphite and MoS_2, were shown to be unstable in the planar from and fold on themselves forming seamless hollow structures like multiwall nanotubes and fullerene-like nanoparticles. The present concise *tutorial review* reports on the salient developments in this field over the last several years. Numerous applications for such nanophases have been proposed, like solid lubricants, ultra-strong nanocomposites, catalysts, *etc.*

I. Introduction

Inorganic nanotubes (INT) and fullerene-like (IF) nanoparticles are hollow closed structures, which are usually produced from compounds with layered (2D) structures, like MoS_2[1–3] and BN.[4] It was argued that, in analogy to carbon fullerenes, nanoparticles of such compounds suffer from inherent chemical instability in the planar form due to their abundant rim atoms. This chemical instability is alleviated by folding and the formation of seamless hollow nanoparticles, which are nevertheless elastically strained. In several cases, the structure and growth mechanism of the IF and INT were elucidated in some detail. These kinds of nanoparticles are currently the subject of a rather intense research.

There has been much progress in the synthesis, structural elucidation, study of the physical and chemical properties and potential applications of IF and INT. Numerous new kinds of nanotubes and nanoparticles have been synthesized in recent years. Among them the synthesis of core–shell nanotubes, such as $PbI_2@WS_2$,[5] the so-called MoS_2 mama-tubes[6] and others have been recently described. The synthesis of macroscopic amounts of INT-WS_2[7] using a fluidized bed reactor has been reported recently. Also important is the synthesis of nanotubes based on 3D compounds which was reviewed in ref. 8. Noteworthy are the spinel $ZnAl_2O_4$ nanotubes prepared through the Kirkendall effect, which were the first ternary (crystalline) nanotubes to be reported.[9] A high-temperature induction furnace proved to promote nanotubular growth of 3D materials, like those of AlN.[10] Aberration (*Cs*)-corrected TEM[11] and DFT calculations[12] of IF and INT brought about significant progress in understanding the structure, growth mechanism and physical behavior of both IF and INT. The mechanical properties of INT-WS_2 were found to defy the conventional wisdom, where the failure of strained samples is determined by the statistics of defects (weak links). Instead, these nanostructures were shown to exhibit an elastic behavior

[a] *Weizmann Institute, Rehovot, Israel. E-mail: reshef.tenne@weizmann.ac.il*
[b] *Hebrew University - Hadassah, Faculty of Dental Medicine, Jerusalem, Israel*

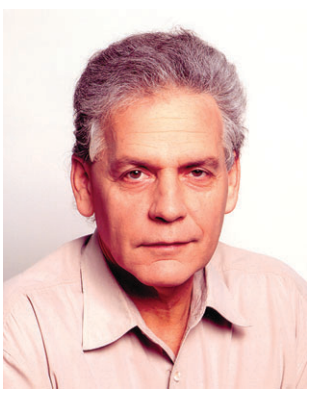

Reshef Tenne

Reshef Tenne earned his PhD in 1976 (Hebrew University). He joined the Weizmann Institute in 1979, where he was promoted to professor in 1995. He headed the Department of Materials and Interfaces and was the director of the Schmidt Minerva Center (2001–2007) and the Helen and Martin Kimmel Center for Nanoscale Science (2003–). He holds the Drake Family Chair in Nanotechnology (2004–). He received the MRS Medal (2005); The Kolthoff Prize of the Technion (2005); Israel Vacuum Society Science Prize (2005); Landau Prize in Nanotechnology (2006); MRS Fellow; the Israel Chemical Society Prize and the Advanced Research Grant (ERC) in 2008.

Meir Redlich

Meir Redlich received his DMD in 1980 (Hebrew University). He became specialist in Orthodontics (Cum Laude) in 1994 (Hebrew University). In 2001 he earned a PhD in Oral Biology (Hebrew University). He joined the department of Orthodontics in Hadassah Medical Center-Hebrew University in 1998, where he was promoted to senior lecturer in 2004. Since then he is the director of research activities in the department. He was the director of the postgraduate program in Orthodontics (2003–2006). During the last decade he gained multiple national and international research grants.

almost to the point where the chemical bond fails.[13] Stable IF- and INT-MoS_2 suspensions were obtained by their surface functionalization with a Ni-chelating agent.[14] This progress made it possible to explore many of the IF properties in different solutions.

Numerous kinds of applications were proposed for the INT and IF. In particular, IF-WS_2 (IF-MoS_2) were shown to exhibit superior tribological properties.[15] Indeed, following an intensive R&D effort a number of products based on formulated oils and greases were launched last year with many others on the way to the marketplace. Furthermore, metallic coatings impregnated with IF nanoparticles have been studied and their self-lubrication behavior was investigated, in particular for medical applications.[16] These self-lubricating coatings were also recently commercialized. The addition of small amounts (<1%) of *e.g.* IF-WS_2[17] and BN nanotubes[18] to various polymer matrices led to nanocomposites with superior mechanical properties, like strength and fracture toughness. It is believed that in the next few years new IF-based nanocomposites with favorable mechanical properties will be developed and eventually commercialized.

The present review paper will focus on recent progress in the synthesis, structural elucidation, and the study of the physical and chemical properties of crystalline IF and INT. Also, much progress has been achieved in recent years with the synthesis and the study of polycrystalline nanotubes. Such nanotubes are generally prepared *via* anodization of metallic foils; template synthesis and related "chemie douce" methods. For example, arrays of polycrystalline TiO_2 nanotubes have been fabricated by anodization of Ti foils and are being intensively studied for, *e.g.* photocatalytic degradation of pollutants and photoanodes in dye-sensitized solar cells. This important subject has been thoroughly discussed in several recent review papers, like ref. 9 and will not be further elaborated here. This review is intended to give a brief overview of the current efforts in the field of crystalline IF and INT and therefore, except for a few references, all the cited literature pertains to the last three years.

Furthermore, a number of directions in the development of new technologies and products based on IF and INT will be described. In particular, medical technologies which are based on the beneficial tribological and mechanical behavior of the IF nanoparticles and INT will be presented and their future prospects will be briefly discussed.

II. Recent progress with INT and IF synthesis

A few recent examples of the extensive work done in this field will be presented. Perhaps the most significant accomplishments in the field are the early mechanistic studies which permitted the recent scaling-up of the synthesis of IF- and INT-WS_2.[8] These mechanistic aspects have been discussed extensively in earlier papers and review articles and will not be further rehearsed here. Two growth mechanisms for INT-WS_2 from tungsten oxide powder and H_2S have been proposed: 1. In the first step, $W_{18}O_{49}$ nanowhiskers are grown and are subsequently converted into multiwall WS_2 nanotubes by reacting them with H_2S and H_2 gasses. The (sulfidization) reaction occurs from the outwards in and consequently is dictated by the slow diffusion of sulfur from the surface of the nanotube inwards towards the core. The synthesized nanotubes can be many tens of microns long and with fairly big (30–150 nm) diameters, *i.e.* >20 WS_2 walls. 2. According to the alternative mechanism, the multiwall nanotubes grow almost instantaneously having no solid oxide template in the core. They are rather slender (15–30 nm in diameter) and contain anywhere between 4 and 8 walls. Unfortunately, these latter kind of WS_2 nanotubes have not been grown in large amounts and in a pure form, so far.

In another progress, scaling up of the synthesis of IF-MoS_2 nanoparticles to gram quantities was recently reported (Fig. 1a).[20] In contrast to the IF-WS_2 nanoparticles, the newly synthesized IF-MoS_2 nanoparticles appear to have an oval shape and possess a compact multiwall structure (>20 walls, in general) with a tiny hollow core in the center (consider Fig. 1b). This advancement allowed for a detailed tribological experimentation of the nanoparticles (*vide infra*). Future work will attempt to make IF-MoS_2 powders alloyed with other elements which will endow those nanoparticles interesting physical properties.

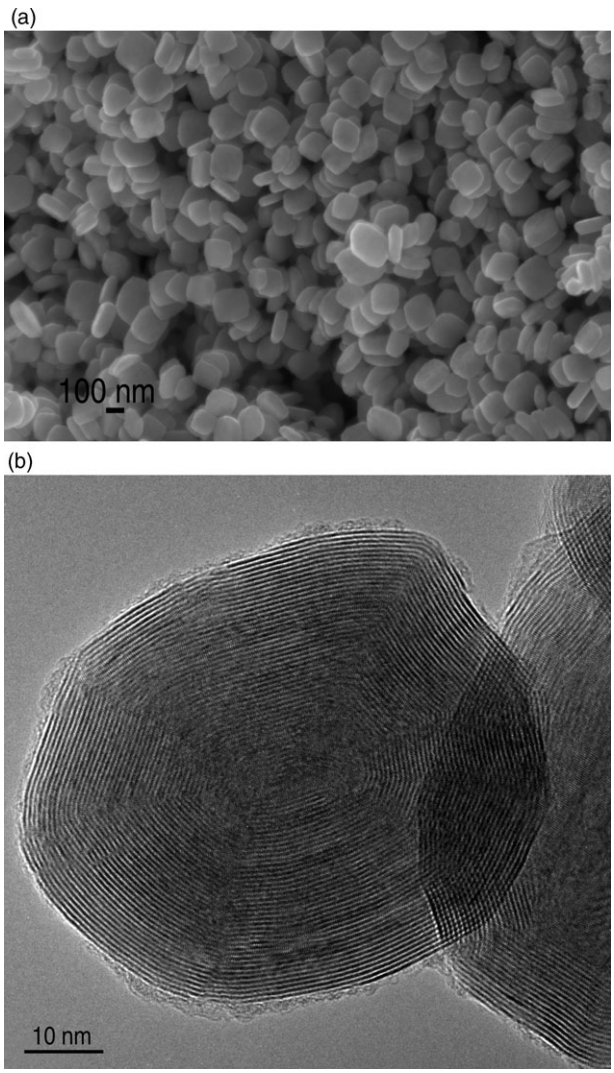

Fig. 1 (a) SEM micrograph of a typical assortment of IF-MoS_2 nanoparticles (courtesy of Dr R. Rosentsveig); (b) TEM micrograph of a single IF-MoS_2 nanoparticle (courtesy of Dr R. Popovitz-Biro).[15]

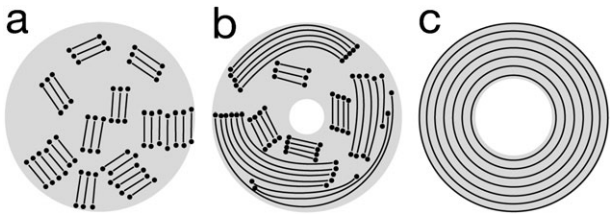

Fig. 2 Schematic representation of the process of crystallization and formation of a hollow IF-WS_2 nanoparticle by *in situ* heating of amorphous WS_x nanoparticles in the TEM.[21] In (a) the first WS_2 nanocrystallites are formed. They are misoriented with respect to each other and they possess a lot of dangling bonds at their edges, which are symbolized by points. In (b) the WS_2 crystallites undergo coarsening and they reorient themselves along the contour of the spherical nanoparticle. This process is terminated in (c), where hollow closed IF-WS_2 nanoparticles are formed with complete annihilation of the reactive dangling bonds.

Another remarkable observation was done by making use of TEM with an *in situ* heating stage.[21] First, amorphous WS_x nanoparticles were obtained in a separate set-up by the gas-phase reaction between tungsten carbonyl and sulfur. These nanoparticles were heated to 800 °C in the TEM. Gradual formation of tangential WS_2 layers and healing of defects led to coalescing and eventually to closed sheets, *i.e.* IF-WS_2. The salient features of this process are captured by the schematic representation in Fig. 2. The crystallization process was shown to start at the outer surface of the round nanoparticle and propagate inwards. This observation could indicate that during the heating of the amorphous nanoparticles, surface excess sulfur is lost and stoichiometric WS_2 is formed. The heated outer surface loses sulfur first and crystallizes and the process advances inwards along the temperature gradient. A similar process was found to occur in IF-MoS_2, nonetheless at somewhat lower temperatures.

A most remarkable progress was recently realized by Tremel and co-workers, where molten Bi nanodroplets were used as a catalyst for the promotion of SnS_2 nanotubes growth *via* a vapor–liquid–solid (VLS) mechanism.[22] Here, the vapor-phase reactants required for the nanotube growth are formed by heating solid SnS_2 nanoflakes to 800 °C. An inert carrier gas provides the required dilution of the vapor-phase species. This development opens a new route for the synthesis of inorganic nanotubes of 2D compounds.

The availability of quite perfect WS_2 nanotubes in substantial amounts, offered the opportunity to use them as templates for the growth of core–shell nanotubular structures, and was first realized for PbI_2@WS_2 core–shell nanotubes.[5] Given their relatively large hollow core (8–12 nm) it was postulated that molten salts of compounds with genuine layered (2D) structure will be sucked inside into the hollow stem by capillary forces and wet the inner walls of the template. Upon fast cooling they would form folded-closed layers giving rise to such core–shell nanotubular structures (see Fig. 3). The intensity analysis of the nanotube (see Fig. 3) clearly reveals a spacing of 0.6/0.7 nm for the interlayer distance of the outer (6)/inner (3) layers typical for WS_2/PbI_2 core–shell nanotubes. The imbibition of a molten drop of PbI_2 into the hollow core of MoS_2, BN and carbon nanotubes was

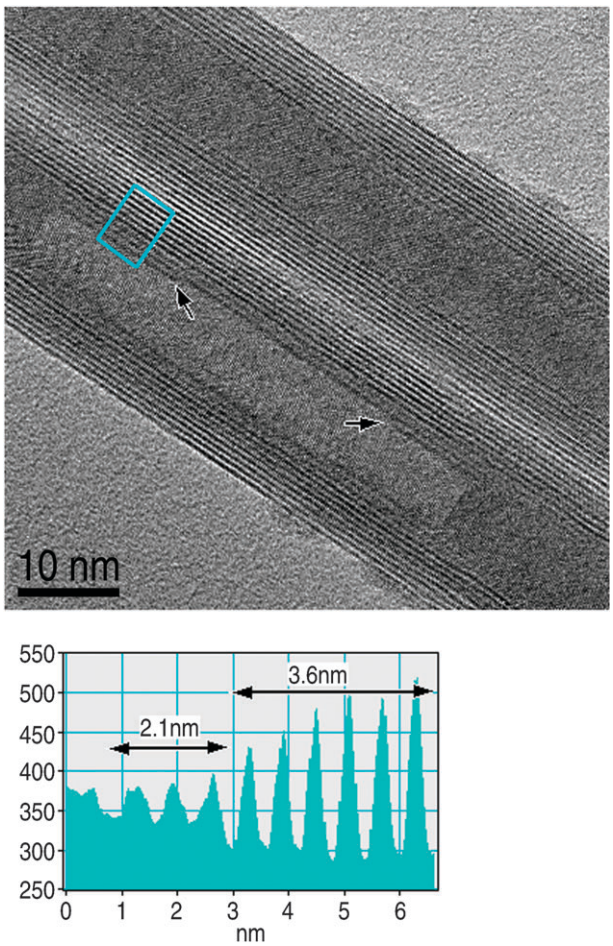

Fig. 3 TEM analysis of PbI_2@WS_2 core–shell nanotubes (courtesy of Dr R. Popovitz-Biro).[6]

recently studied by molecular dynamics calculations.[23] The molten PbI_2 molecules were shown to wet the MoS_2 inner walls and arrange themselves into a shell model, reminiscent of the layered solid. The number of layers of the inner nanotube (PbI_2) was limited to no more than three due, most likely, to the high elastic strain required to form curved structures of diminishing radius. Furthermore, so far the yield of the process was not very high. Obviously, the choice of compounds which can form similar core–shell structures is limited to those with melting point no higher than *ca.* 600 °C, or else a chemical reaction between the host and guest may occur. Other layered compounds with low melting points, like BiI_3 and AsI_3 were shown to form core–shell nanotubular structures by a similar process.[24] Surface tension of the molten compound is likely to play an important role in the imbibition of the salt into the hollow core of the nanotube.

While various core–shell nanotubular structures with 2D metal-di(tri)iodides were prepared using WS_2 nanotubes as templates, no analogous structures could be obtained with 2D metal dichlorides or dibromides, so far. The difficulties may lie in the larger ionicity of the latter compounds, which prevents wetting of the WS_2 nanotube inner walls to form conformal coatings of the template surface. Furthermore, the metal dichloride compounds are very hygroscopic and they can not

be easily handled. More work is needed to clarify these points. Compounds, like CsI, which crystallize in a CsCl (3D) lattice structure, were shown to form nanowire-like structures within the hollow core of the WS_2 nanotube template.

Alternative ways to use the WS_2 as a template for synthesizing a variety of other core–shell nanostructures have been proposed. In particular, using the gas-phase reaction between $MoCl_5$ and H_2S in the presence of the WS_2 nanotubes, WS_2@MoS_2 core–shell structures were obtained in large (>50%) yields. Here a fast, kinetically controlled, reaction occurs on the outer surface of the WS_2 nanotube template. A conformal coating of the nanotubes surface leads to the formation of a few closed MoS_2 layers giving rise to the new core–shell nanotube structure. Is there a limiting factor to the growth of such conformal MoS_2 layers? Is the thickness of the top MoS_2 nanotube dictated by stability or kinetic criteria? More research is obviously needed to address these and other pending questions. There are numerous intriguing questions regarding the physical and chemical behavior of such core–shell nanotubular structures remaining to be addressed. Here detailed theoretical analysis and *ab initio* calculations are called for. For example the broken symmetry at the interface between the two (core and shell) nanotubular structures may lead to new kind of charge- or exciton-confinement, or new Raman modes which have not been observed before.

The synthesis of crystalline nanotubes from compounds with quasi-isotropic (3D) structure has been demonstrated quite recently and showed substantial progress over the past few years. A recent review and a feature article were dedicated to some aspects of this subject.[8,25] Silicon nanotubes have been grown by using germanium nanowires as a template.[26,27] In the first step Ge nanowires were grown by vapor–liquid–solid type growth using gold nanoparticles as the catalyst. Subsequently, a conformal Si film was applied onto the germanium nanowires. Finally, the germanium core was removed by a selective etching in H_2O_2/H_2SO_4 (piranha) solution. The nanotubes grow along the ⟨111⟩ axis and possess a hexagonal cross-section reflecting the symmetry of the Si lattice. The resonance frequency (*ca.* 10 MHz) of the Si nanotubes was measured with the notion of using them as ultrasensitive resonant mass sensors.[27] Other potential applications, including electrically addressable nanofluidic sensors have been discussed.[26] In a related work the first metal silicide nanotubes made of V_5Si_3 were synthesized.[28] The nanotubes were prepared by heating VCl_3 powder at 700 °C and placing downstream a silicon powder and vanadium foil at 950 °C. As expected the V_5Si_3 nanotubes, grown on the vanadium foil, exhibited a hexagonal cross-section reflecting the hexagonal *P*63/*mcm* symmetry of the bulk lattice.

A few more examples of recent progress in the synthesis of crystalline nanotubes of 3D compounds are provided, *e.g.* MgS[29] and CeO_2.[30,31] MgS nanotubes were produced by reacting MgB_2 and GaS in a high-temperature (1600 °C) induction furnace. The high-temperature decomposition of the GaS leads to the condensation of Ga droplets which serve as the catalyst for the growth of the crystalline MgS nanotubes. The hydrogen-storage capacity of the MgS nanotubes attained the value of 2.2 wt% under a hydrogen pressure of ~33.6 atm. With regards to the CeO_2 nanotubes,[30] first rodlike $Ce(OH)CO_3$ was prepared by reacting cerium nitrate with urea at 80 °C for 24 h. The solid product was then mixed with NaOH solution and was reacted hydrothermally at 120 °C for 24 h. The proposed growth mechanism of the crystalline CeO_2 nanotubes is as follows: first the NaOH reacts with the surface of the $Ce(OH)CO_3$ and converts it into $Ce(OH)_3$. This compound possesses a layered structure, and hence its nanosheets can easily enfold the original nanorods. In the high-pH environment, the closed $Ce(OH)_3$ layer is gradually converted into a $Ce(OH)_4$ top film. Meanwhile, the sodium hydroxide etches away the inner core of $Ce(OH)CO_3$ leaving a hollow nanotube. In the final step of drying, the $Ce(OH)_4$ film is deprotonated becoming crystalline CeO_2 nanotube. CeO_2 is a well known catalyst which is used for converting the effluent CO into CO_2 in the auto gas-exhaust. Indeed the CeO_2 nanotubes were tested as catalytic material in the above reaction and were found to be appreciably (three-times better at 250 °C) more efficient than the bulk material. In another study,[31] polycrystalline CeO_2 nanotubes were prepared by electrochemical deposition into porous alumina membrane. The nanotube material showed 400 times increase in the catalytic oxidation of CO at 200 °C as compared to polycrystalline cerium oxide.

While much of the work presented above is carried out at high (>500 °C) temperatures, there has been much progress with the use of "chemie douce", *i.e.* low-temperature syntheses, for the production of IF and in particular INT. Both hydrothermal and sol–gel syntheses have been skillfully employed to synthesize a variety of new kinds of nanotubes. A recent example demonstrating the pros and cons of the low-temperature procedures, is shown in the synthesis of Bi_2S_3 nanotubes.[32] Here, bismuth nitrate ($Bi(NO_3)_3{\cdot}5H_2O$) and sulfur powder (S) were used as the precursors and octadecylamine (ODA) as the solvent. The synthesis was carried out at 100 °C and subsequently the mixture was heated to 200 °C for 10 min. After filtration the product was collected and analyzed. Multiwall Bi_2S_3 nanotubes 20 nm in diameter and 160 nm long were obtained. After 30 min at 200 °C the product converted to Bi_2S_3 nanorods, indicating the relatively modest kinetic stability of the synthesized nanotubes. Another example is provided by the synthesis of ultra-thin Sb_3S_2 nanotubes in a low temperature (175 °C) solution-based reaction.[33] The slender nanotubes were rather short (up to 300 nm). Both Bi_2S_3 and Sb_2S_3 nanotubes could be very useful as thermoelectric materials. In another recent example $ReSe_2$ nanotubes were synthesized.[34] The $ReSe_2$ nanotubes have been synthesized in a sequence of two steps. In the first step, selenium nanotubes were synthesized in a water–ethylenediamine mixture. In the second step, the synthesized Se nanotubes were reacted with ammonium perrhenate [NH_4ReO_4] in ethanolic medium, under solvothermal conditions at 135 °C for 6 days. Beautiful rectangular nanotubes of $AgIn(WO_4)_2$ with a diameter ranging between 80 to 120 nm and length of up to 2 micron were obtained by hydrothermal synthesis.[35] Following Pt loading, photocatalytic hydrogen reduction of these nanotubes was demonstrated using UV light excitation. The normalized photocatalytic reactivity of the nanotubes superseded both the bulk material and TiO_2 nanoparticles (P-25). In general, however, nanotubes synthesized at low

temperatures are shorter and structurally less perfect than those obtained in high temperature synthetic processes. This adverse effect has deleterious consequences on the mechanical and electronic performance of such nanotubes.

In another study, a low-temperature reaction between $Gd(NO_3)_3$ and ammonia solutions at 75 °C and pH 10 was used to synthesize quite uniform and crystalline $Gd(OH)_3$ nanotubes ($P63/m$ symmetry group).[36] By adding $Eu(NO_3)_3$ to the solution and calcination of the product at 600 °C, europium-doped Gd_2O_3 nanotubes which produced intense red emission (610 nm) under UV excitation were obtained.

Most recently, a new strategy for the preparation of heterojunction (amorphous) nanotubular structures was reported.[37] Here, silicon nanowires were grown first as template. Using atomic layer deposition and a series of processes, a physical junction between SiO_2 and Al_2O_3 nanotubes was established. The tips of the nanotubes were connected to metallic electrodes and were immersed in a nanofluidic device. By proper tuning the pH of the solution a most remarkable ionic diode effect could be demonstrated in KCl solution.

III. Chemical and physical behavior of inorganic fullerene-like nanoparticles and nanotubes

III.a Considerations of the stability of inorganic nanotubes and fullerene-like nanoparticles

The recent progress with high flux and far from equilibrium synthesis of hollow nanostructures shed new light on a number of issues, not dealt with before. A very important one is that of the smallest hollow MoS_2 nanoparticles. A series of recent publications combining laser ablation of MoS_2 targets, electron microscopy and *ab initio* calculations clarified some of the complicated issues. As shown in Fig. 4, the hitherto unknown phase behavior of Mo and S in the nano-range, or else stated the genesis of bulk MoS_2 from the elements, started to clarify once the phase behavior of small Mo–S clusters became apparent. It was clearly determined that below a few hundreds atoms, the trigonal prismatic Mo–S bond is unstable. Rather clusters of the type Mo_4S_6 and Mo_6S_8 made of inner Mo polyhedra and flanked by sulfur polyhedra are stable below *ca.* 100 atoms. Multiwall MoS_2 nanooctahedra, made of six symmetrically disposed rhombi (and two missing sulfur atoms) in the corners become stable between 10^3–10^5 atoms (3–7 nm in size) and are indeed the smallest hollow closed structures, *i.e.* the genuine MoS_2 fullerenes.[11,38,39] Beyond that size and probably up to about 10^7 atoms (*ca.* 20–200 nm), the nanotubes (INT) and the quasi-spherical (fullerene-like-IF) MoS_2 nanoparticles become stable. Bulk 2H-MoS_2 platelets become the most stable species at still larger sizes (> 0.3 micron). Obviously, one finds 2H-MoS_2 platelets smaller than 100 nm and IF nanoparticles larger than 0.2 micron. However, strictly speaking such nanoparticles are the aberration rather than the rule.

The strain energy/atom varies usually as $1/R^2$, where R is the radius of the nanotube. For a given diameter, the strain in MoS_2 nanotubes is about one order of magnitude larger than that for carbon nanotubes (see Fig. 5). To alleviate the strain effects, typically MoS_2 nanotubes come in larger diameter (> 15 nm) as compared with carbon nanotubes (typically 1.5 nm). Furthermore, it has been shown that the van der Waals interaction between the molecular sheets promotes the stability of multiwall (5–10 layers) nanotubes. However, given the fact that the van der Waals interaction is appreciably weaker than the Mo–S bond energy, it was hypothesized that high-temperature synthesis followed by rapid quench will favor single (or double) wall nanotubes and fullerene-like nanoparticles. Indeed, using the focused solar beam irradiation of a MoS_2 target (*ca.* 2000 °C), single-wall nanotubes have been obtained (see Fig. 6), though with quite poor reproducibility.[40] It is anticipated that by adding a catalyst or modifying the growth conditions, such nanotubes would be produced in the future in substantial amounts.

In contrast to carbon and MoS_2 nanotubes, imogolite nanotubes are asymmetric along the *c*-axis. This asymmetry

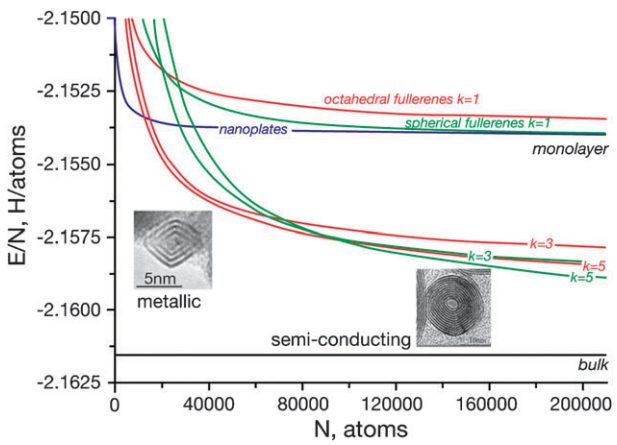

Fig. 4 The dependence of the energy per atom E_t/N on the total number of atoms N for various MoS_2 nanostructures: triangular nanoplatelets (blue); octahedral fullerenes with k shells (red), and spherical fullerene-like nanoparticles (green) with k shells (adapted with the permission of Wiley-VCH from ref. 38).

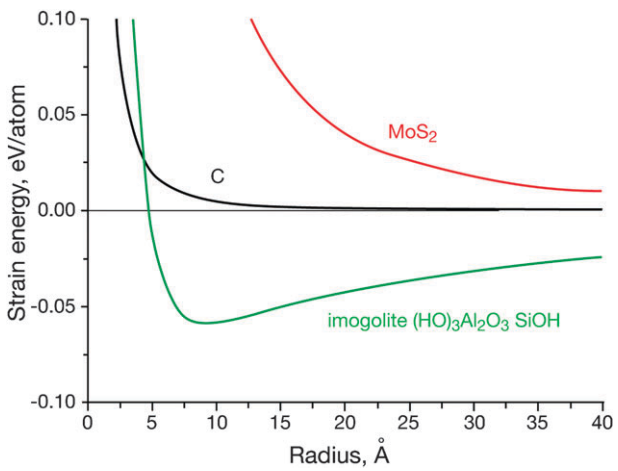

Fig. 5 Graph showing the calculated elastic energy/atom as a function of (zig-zag) nanotube diameter for carbon, MoS_2 and imogolite nanotubes. The fundamentally different driving force for closure of the symmetric carbon and MoS_2 nanotubes compared to that of the (asymmetric) imogoloite nanotubes is clearly revealed in this picture (courtesy of Prof. G. Seifert).

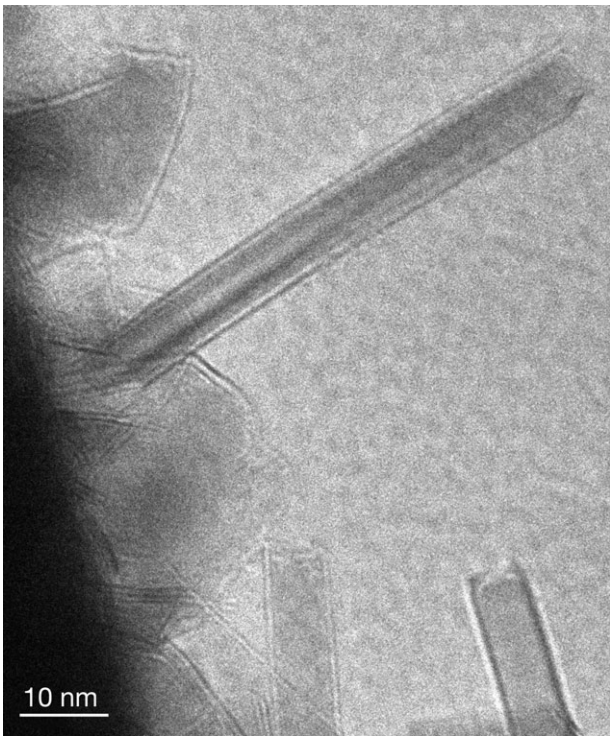

Fig. 6 TEM image of a single-wall MoS_2 nanotube produced by solar ablation (courtesy of Dr Ana Albu-Yaron).[40]

stems from the fact that the outer alumina octahedra in the molecular sheet are larger than the inner silica tetrahedra.[41] This size difference leads to a built-in strain in the sheet and dictates a minimum in the strain energy/atom for (12,0) nanotubes.

III.b Chemical manipulation of inorganic nanotubes

In analogy to nanoparticles of different sorts, like quantum dots and carbon nanotubes, the chemical modifications of IF and INT surfaces is a key step in affording stable suspensions of these nanoparticles and blending them in different polymers. The functional ligand consists of an anchor group that attaches to the nanoparticle surface and a tail which renders them soluble in various solvents. Also, the tethered molecules allow the nanoparticles to disperse well in polymer blends or oil suspensions. For example, attached alkyl chains make the nanoparticles soluble in nonpolar solvents, while deprotonated carboxylic or alkyl amine functions makes them soluble in water or other polar solvents. So far, not much work has been dedicated to this important topic. An early effort appears in ref. 14. Here, a nitrilotriacetic acid (NTA) group was used to chelate Ni^{3+} ions from above. The partially empty coordination sites of the nickel ions were shown to bind to the outermost sulfur atoms on the surface of the IF (INT)-WS_2 nanoparticles. On its opposite side, the NTA moiety was linked to a polymer [poly(pentafluorophenyl acrylate)] which terminates with polar groups such as catechol (1,2-dihydroxybenzene) (see Scheme 1). Such surface-functionalized IF-WS_2 nanoparticles formed stable suspensions with water. Furthermore, decoration of TiO_2 nanowires with surface-functionalized IF nanoparticles was accomplished using this methodology. In a similar vain,

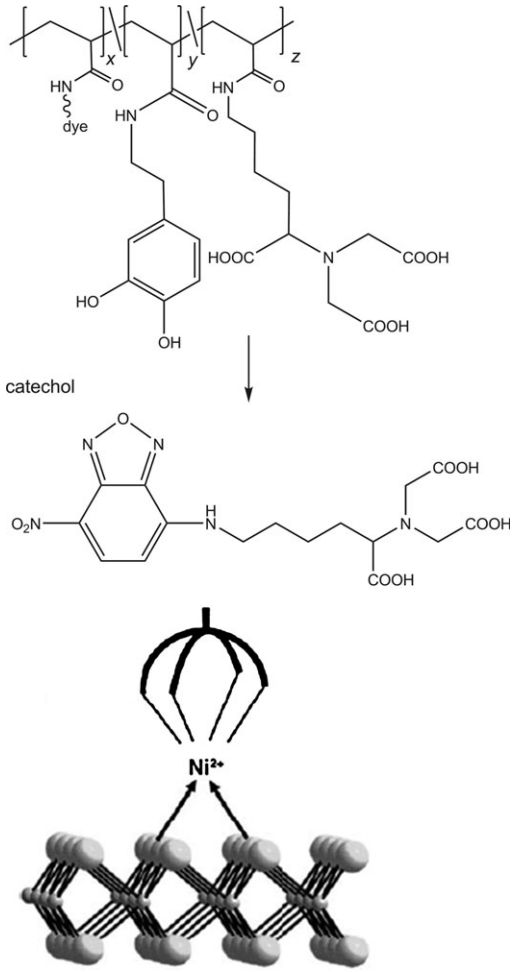

Scheme 1

BN nanotubes were surface functionalized by the tetra-potassium salt of tetracarboxylic acid perylene-3,4,9,10-PTAS (see Scheme 2).[42] The functionalization of the nanotubes with the PTAS moiety led to the formation of stable suspensions in aqueous solutions (0.3 mg mL^{-1}). The strong attachment of the PTAS molecules to the BN nanotube surfaces is formed through π–π interactions. The solubility of the BN nanotubes in

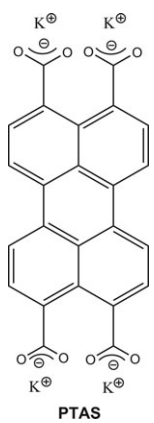

Scheme 2 PTAS = perylene-3,4,9,10-tetracarboxylic acid tetra-potassium salt.

aqueous solution opened various possibilities, *e.g.* to blend the BN nanotubes in various nanocomposites and for drug delivery.

Another very important and promising strategy is the intercalation of inorganic nanotubes with a variety of metals and nucleophilic groups. Reversible intercalation of foreign atoms and molecular moieties may lead to their applications in intercalation (rechargeable) batteries; drug delivery; remediation of water and for detectors/sensors. A recent example is the gas-phase intercalation of Na, K and Rb atoms in fullerene-like nanoparticles of WS_2 (IF-WS_2).[43] The $c/2$ lattice spacing between the layers was shown to significantly expand upon intercalation. However, due to the substantial lattice strain, this lattice expansion (0.81 nm) is limited to the outermost layers (see Fig. 7). The innermost closed WS_2 layers remain unchanged (0.62 nm). Furthermore, XPS measurements showed that the Fermi energy of the intercalated IF nanoparticles moved upwards, endowing them with n-type character.

Insertion of potassium and chloride ions into the interlayer spacing of magnesium hydrosilicate ($Mg_3Si_2O_5(OH)_4$)

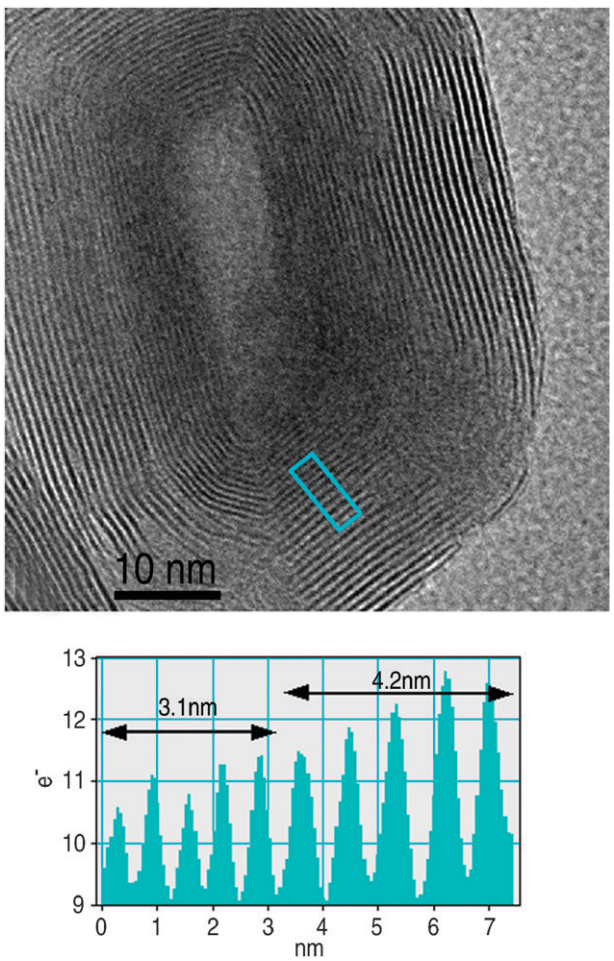

Fig. 7 TEM image of an individual IF-WS_2 nanoparticle which was partially intercalated with rubiduim atoms. Note that due to the significant strain, the intercalation which is indicated by lattice expansion (0.64 nm) of the closed shells is limited to the outermost 15 layers. The innermost layers of the nanoparticle exhibit the regular lattice spacing (0.62 nm) (Reprinted with permission from ref. 43. Copyright American Chemical Society, 2008).

nanotubes was also recently demonstrated.[44] Here the nanotubes were added to KCl solution, and a spontaneous insertion of the foreign atoms into the van der Waals gap of the nanotubes was accomplished within 24 h. Obviously, intercalation of this kind is effective in cases where both the nanotubes and the guest moieties are compatible with aqueous solutions, or other solvents. Since the walls of the nanotubes and fullerene-like nanoparticles are chemically very inert and quite impermeable, the diffusion of the guest moiety depends on the availability of weak links, *i.e.* surface defects or open tips at the nanotube edges. However, when the nanotube is not fully crystalline and its walls are made of small crystallites, the fast intercalation kinetics garners rapid charge/discharge cycles and high capacity for the guest atoms. This idea is well demonstrated in *e.g.* the case of Co_3O_4 nanotube arrays, which grow topotactically from β-$Co(OH)_2$ nanowires.[45] Here, fast Li intercalation and high electrical capacity (1000 mAh g^{-1}) was achieved for the first 30 charge/discharge cycles with gradual decay to 500 mAh g^{-1} after 80 cycles.

Hexaniobate nanoscrolls (NS-$H_4Nb_6O_{17}$) were synthesized and used in photocatalytic assemblies for H_2 production. Here, ethylenediaminetetraacetic acid (EDTA) served as a sacrificial electron donor and platinum (Pt) nanoparticles as catalysts.[46] $Ru(bpy)_3^{2+}$ and $Ru(bpy)_2(4,4'\text{-}(PO_3H_2)_2bpy)^{2+}$ (bpy = 2,2′-bipyridine) were employed as visible-light sensitizers (abbreviated as Ru^{2+} and RuP^{2+}, respectively). RuP^{2+}, which is anchored by a covalent linkage to the NS-$H_4Nb_6O_{17}$ surface, functions more efficiently than the electrostatically bound Ru^{2+} complex. RuP^{2+}-sensitized NS-$H_4Nb_6O_{17}$ produced H_2 photocatalytically using visible light ($\lambda > 420$ nm) with initial apparent quantum yields of 20–25%. At the optimum sensitizer concentration and Pt loading, the photochemical hydrogen evolution process was shown to be primarily limited by the light absorption efficiency and charge injection from the photoexcited sensitizer into the oxide semiconductor particles. The enhancement of the catalytic oxidation of CO into CO_2 by CeO_2 nanotubes has been discussed before.[30,31] Although direct comparison between the two works is difficult, the polycrystalline nanotubes, as expected, seem to be more reactive[31] than the crystalline ones.[30]

III.c Mechanical properties

Progress with the synthesis of new inorganic nanotubes and fullerene-like nanoparticles opened a vast number of opportunities to chemically and physically manipulate these new nanostructures in order to obtain new functionalities which are not amenable with bulk materials. For example, the mechanical properties of such nanotubes were recently shown to be remarkably different from the bulk materials. The mechanical behavior of bulk materials is dictated by the nature of the chemical bond holding the atoms together as well as structural and chemical defects. Intrinsic defects, like vacancies, interstitial or antisites, are dictated by the thermodynamics of finite temperature systems. On the other hand extrinsic defects, like grain boundaries and dislocations are induced by the processing of the material. Therefore, most bulk materials are appreciably weaker than what would be predicted by considering the strength of their respective chemical bonds.

In contrast to this, a series of experiments with individual multiwall WS_2 nanotubes[13] have clearly indicated that their mechanical properties are predictable from first principle calculations, *i.e.* they can be referred to the strength of the chemical bond. Fig. 8a shows a snapshot taken during a tensile test of an individual WS_2 nanotube, while Fig. 8b shows the stress–strain curve of this nanotube. The nanotube showed elastic (linear) behavior almost to failure. The Young's modulus calculated from the slope of the curve; strength and strain at yielding are: 160 GPa, 17 and 10%, respectively. Some 50% of the measured nanotubes showed strength in excess of 13 GPa which is indicative that they are basically free of critical defects. Density functional tight binding (DFTB) calculations of single-wall MoS_2 nanotubes were carried out and were compared (after normalization) to the experimental data of WS_2 nanotubes. The normalized (from MoS_2 to WS_2) calculated data was about 30% higher than the experimentally observed strength and strain to failure. Furthermore, the theoretical calculations clearly show that under extreme strain one of the Mo–S bonds in the middle of the nanotube fails, which leads to stress concentration on the neighboring bonds and to their rapid failure. This mode of failure does not involve any intrinsic or extrinsic defect. Future work may focus on mechanical testing of individual nanotubes within the TEM, which may shed light on the atomic structure of the nanotubes under strain and their failure. Furthermore, coupling between optical, electrical and mechanical measurements can give rise to unexpected results.

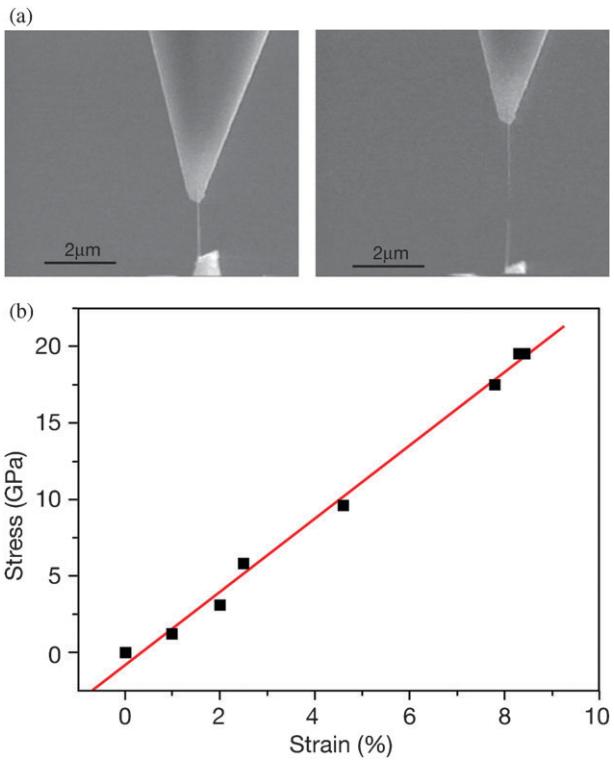

Fig. 8 (a) SEM images of a WS_2 nanotube during a tensile test before (left) and after (right) failure; (b) Strain–stress curve of such a nanotube (courtesy of Dr I. Kaplan-Ashiri) (Reprinted with permission from ref. 13. Copyright the National Academy of Sciences, 2006).

In another series of experiments,[47] individual WS_2 nanotubes were suspended on an empty channel and were pushed sideways in the middle (bending test). The sliding of one nanotube layer with respect to its neighbors could be calculated from the modified Timoshenko's bending equation. In bulk materials the ratio between the Young's (E) and shear (G) moduli is high (about 0.3). Consequently the contribution of the shear mode to the bending energy is rather small. The relatively free sliding, *i.e.* the low sliding modulus ($G/E \sim 0.01$) of neighboring walls with respect to each other in the nanotube, allows this mode to take a relatively significant share ($> 10\%$) of the bending energy. These studies together with the advent of the large-scale synthesis of fullerene-like WS_2 and its nanotubes[8] are nourishing a new wave of studies aimed at developing IF- and INT-based ultra-high strength nanocomposites of various sorts.

III.d Optical behavior

Resonance Raman ($\lambda_{exc} = 632.8$ nm) spectra of individual MoS_2 and WS_2 nanotubes were recently measured and compared to the bulk materials.[48] An up-shift of the peaks (3–10 cm^{-1}) of both the original A_{1g} (408, 421 cm^{-1}) and E^1_{2g} (383, 356 cm^{-1}) Raman modes was observed. This shift was attributed to the built-in strain in the nanotubes. Indeed, collapsed MoS_2 nanotubes (ribbons) showed no such shift. Furthermore, electron diffraction analysis showed that locally the nanotubes crystallized in the high-pressure rhombohedral (3R) symmetry rather than the hexagonal symmetry, which is the stable polymorph in ambient conditions. In another study[49] the Raman lines of core (W)–shell IF-WS_2 nanoparticles were studied as a function of the hydrostatic pressure in a diamond anvil cell. The A_{1g} line at 420 cm^{-1} was shown to contain a new low-energy shoulder at 416 cm^{-1} which is attributed to two-phonon coupling originating from longitudinal acoustic (LA) and transverse acoustic (TA) phonons at the K-point of the Brillouin zone. This low energy shoulder is enhanced by the curvature of the nanoparticles. The Raman spectra of the core–shell W/IF-WS_2 nanospheres under different pressures are shown in Fig. 9a. It is clearly observed that the intensity ratio of the LA + TA and A_{1g} modes varies noticeably with increasing pressure. This ratio first increases and then reaches a maximum and decreases with the application of a higher pressure, as shown in Fig. 9b. Upon releasing the pressure, the original lineshape is restored indicating that the nanotubes are stable under hydrostatic pressure of up to 18 GPa and could therefore serve to reinforce ultra-high-strength nanocomposites.

The Raman spectra of imogolite $-(HO)_3Al_2O_3SiOH-$ nanotubes were studied.[50,51] The mineral imogolite is found in soils of volcanic origin and is composed of single-wall nanotubes with external tube diameter of 2.3 nm. In contrast to any other kind of nanotube were the elastic energy goes monotonically down with increasing diameter, here a clear minimum is observed. This energy minimum is dictated by the difference in the b-axis of the outer alumina octahedra and the interconnected inner sheet of silica tetrahedra, which induces a bending force on the imogolite layer. Nanotubes are characterized by a mode describing a concerted movement

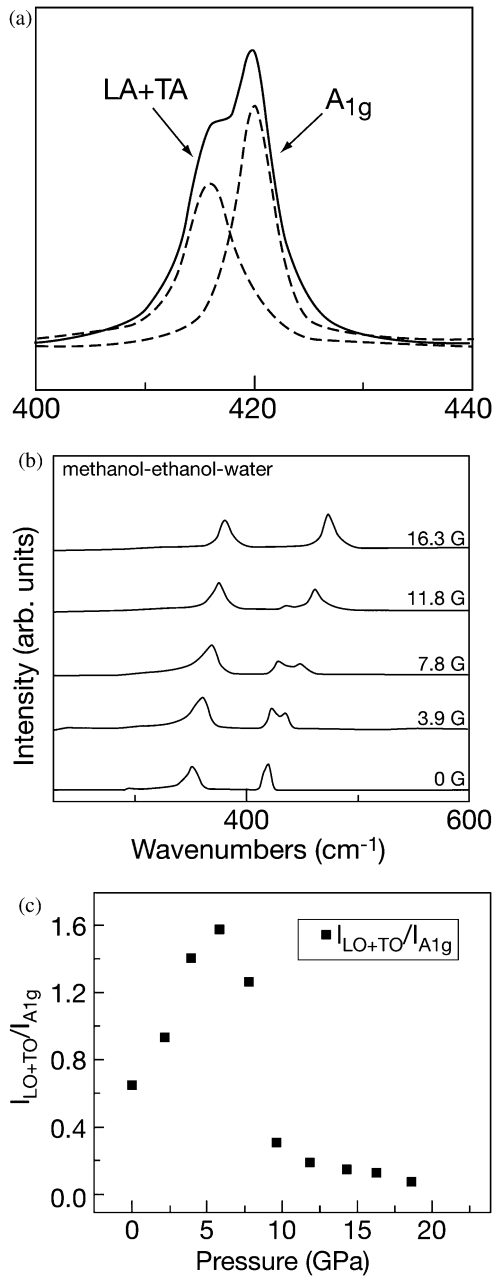

Fig. 9 (a) The evolution of the Raman spectrum of IF-MoS_2 nanoparticles under pressure; (b) Intensity ratio of the LA + TA/A_{1g} peaks (adapted with the permission of the Institute of Physics from ref. 49).

of the atoms, which is referred to as the Raman breathing mode (RBM). This mode has been studied in great detail in carbon nanotubes. The RBM of imogolite nanotubes, which is the first of its kind, was measured and calculated. The energy of this mode goes down with increasing diameter, reaching 54 cm^{-1} for the (12,0) nanotubes, which corresponds to the elastic energy minimum (see Fig. 5).

III.e Electronic structure and transport

While much effort has been devoted to the study of the mechanical properties of IF and INT, the research on the electronic and transport properties of these nanoparticles remained rather scant. A phototransistor based on individual WS_2 nanotubes, which is sensitive to visible light was recently fabricated and tested.[52] The maximal sensitivity of the phototransistor was obtained when the visible light for a halogen lamp was polarized in parallel to the nanotube axis and the minimum sensitivity occurred when the light was polarized perpendicular to the nanotube axis. The carrier mobility and carrier density increased from 4.1×10^{-4} and 1.54×10^{6} in the dark to 1.3×10^{-3} and 2.57×10^{7} V cm^2 s^{-1}, respectively, under illumination. Transistors capable of detecting visible light would have a wide range of applications in consumer and medical electronics.

A most remarkable development of a nanofluidic diode based on a SiO_2/Al_2O_3 nanotube heterojunction was recently demonstrated.[36] At a neutral (7) pH of the solution the surface chemistry of the acidic SiO_2 segment becomes negatively charged while that of the basic Al_2O_3 is positively charged due to adsorbed OH_2^+ groups. For sufficiently low KCl concentrations the Debye length of the solution exceeds the diameter of the nanotube hollow core. Therefore, the positive K^+ ions flow through the SiO_2 segment (p-type), while the Al_2O_3 side permits flow of the negative Cl^- ions (n-type). In the junction zone a concentration gradient maintains the potential drop. Under reverse bias the ions are excluded from the junction zone in the hollow core of the nanotube and the current ceases. Under forward bias conditions, the negative (Cl^-) and positive (K^+) ions flow towards the junction and recombine to KCl molecules which diffuse outside the junction zone. Thus, a rectifier for ion flow has been established using this nanotube junction. This report opens a whole new range of opportunities to fabricate new devices, including logic gates, and plethora of applications.

IV. Applications

IV.a Tribology

While some potential applications of IF and INT have already been discussed for some time, commercial realization of IF-WS_2 as a solid lubricant only started during 2008. There are many issues remaining to be resolved in this context. First, it would be desirable to have the size of typical IF nanoparticles (currently >80 nm) as small as possible. The size of the nanoparticles is important for a number of reasons. First, smaller nanoparticles could make a more homogenous and stable oil suspension; secondly, access into the contact area between the two metal pieces could become easier. Finally, the flow of the nanoparticles in the oil could become more homogenous, too, especially near the surfaces. However, given the built-in strain of the folded structures,[12] it is not easy to foresee a simple solution to this issue. One way to accommodate the strain and reduce the size of the nanoparticles is by producing less than perfect nanoparticles which contain defects, especially in the corners where the strain is highest. However, introducing defects into the nanostructures may compromise their mechanical behavior and therefore their long-term durability. Another possible solution is to synthesize nanoparticles with smaller numbers (<10) of MS_2 layers. Since the elastic energy of folding depends on the thickness

to the power of three, nanoparticles with fewer than 10 layers may have smaller (<50 nm) radii.

Another critical issue is the agglomeration of the nanoparticles, which influences the tribological characteristics and the shelf-life of the suspensions. In order to minimize the agglomeration of the IF and INT a number of synthetic procedures were recently advanced.[14,52] In one such strategy,[53] alkyl silane groups were tethered to the IF-WS_2 nanoparticle surface, probably through surface defects which adsorb water molecules or OH groups. Although the coverage of the nanoparticles surface is less than half, it was clearly observed that the degree of agglomeration has been reduced from a mean size of about a thousand nanoparticles to two hundreds and fewer. The reduced agglomerate size favorably influenced the stability of oil suspensions and the long-term tribological behavior of oils formulated with these surface-functionalized IF nanoparticles. The surface-functionalized IF nanoparticles can be further manipulated in order to endow them with specific chemistries which will allow them to serve in, *e.g.* drug delivery, or photostimulated tumor therapy.

While numerous applications for the nanoparticles suspended in lubricating fluids have been proposed and some are already in use, a variety of other uses could be also envisaged. One such example is self-lubricating surfaces which are obtained by impregnating the IF nanoparticles into various coatings. Thus, electroless/electrodeposition coatings of metallic substrates with nickel–phosphorous and cobalt films impregnated with IF-WS_2 nanoparticles (see Fig. 10) have been demonstrated.[16,54] Here a remarkable reduction in the friction coefficient, as compared to the pure metallic films, was observed. Unexpectedly, the IF nanoparticles seem to also play the role of cathodic protector on the film, by slowing down the oxidation of the topmost metallic layer during the tribological tests.

Nickel titanium (shape-memory) alloys and stainless steel are used extensively in various medical disciplines such as orthopedics, urology, dentistry, cardiovascular therapy *etc.* Orthodontics is a dental speciality that diagnoses, prevents

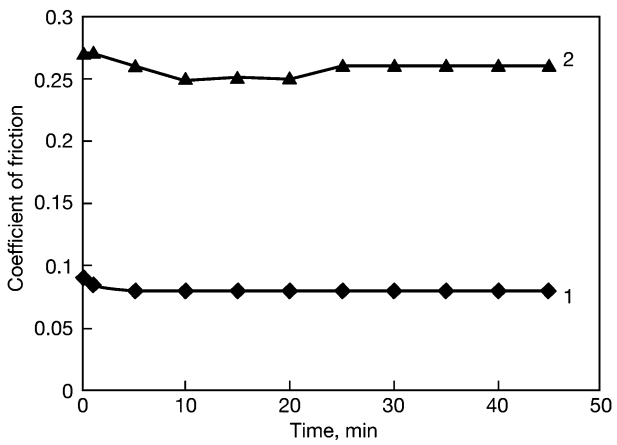

Fig. 10 Comparison between the friction coefficient behavior of NiTi foil coated with electrodeposited cobalt film impregnated with IF-WS_2 nanoparticles (1); and the bare NiTi substrate (2). The tribological tests were performed using a ball-on-flat set-up at a Hertzian pressure of 1.5 GPa and velocity of 0.2 mm s^{-1} (adapted from ref. 54).

Table 1 Testing of stainless-steel orthodontic wires inserted in a bracket in different angulations. Comparison between uncoated and wires coated with Ni–P film impregnated with IF-WS_2 nanoparticles

Angle Coating	0° (N)	5° (N)	10° (N)
Uncoated wire	1.32 ± 0.12	2.95 ± 0.09	4.00 ± 0.19 dry 3.35 ± 0.21 wet
Ni–P + IF coated wire	1.10 ± 0.06	1.58 ± 0.25	1.85 ± 0.21 dry 1.57 ± 0.23 wet

and treats teeth which are not properly located in the jaws. This is done by application of a mechanical load (orthodontic force) on the teeth. This force affects the tissues surrounding the teeth, thereafter enabling their movement. Teeth movement is entirely regulated by nickel titanium or stainless steel wires. The wires are inserted into brackets, which are bonded onto the teeth surface. Unfortunately, the friction between the wire and the bracket leads to the application of an excessive force (>50%). This situation causes undesirable teeth movement; elongating the treatment period; bring about irreversible shortening of the roots of the teeth (root resorption) and causing discomfort to the patients. IF coating of the orthodontic wires brought about a significant reduction of the mechanical force (see for example Table 1[16]) required for moving the teeth. This approach is indeed not unique to orthodontic wires and recent efforts focused on a number of other medical technologies. One of the main concerns in the ongoing use of NiTi alloys for biomedical purposes is the fatigue behavior of the material. During the last few years clinical studies reported removal of urological and cardiovascular stents due to high failure rate of the devices. Fatigue behavior of metallic parts can be affected also by stress-induced rapid diffusion of ambient reactive gasses, like oxygen, through the grain boundaries. Considering the protective role of the IF nanoparticles impregnated into metallic films, it is not unlikely that such coatings will increase the fatigue resistance of the NiTi devices.

Many tribological surfaces can not be coated in wet processes, and vacuum-based techniques are desirable for these cases. The main difficulty in applying such techniques is that they should permit the pristine IF nanoparticles to be co-deposited on the underlying surface with as little damage as possible. Indeed, in a recent work,[55] IF nanoparticles were evaporated onto a substrate by using a cluster evaporation chamber and electromagnetic injector, which was mounted into a magnetron sputtering set-up. Quite uniform films of TiN impregnated with IF-WS_2 nanoparticles were obtained using this technique, as well as films containing other nanoparticles. It is likely that in the future such technologies will be used to manufacture self-lubricating surfaces for a variety of applications in the aerospace; medical and automotive industries.

IV.b Nanocomposites

Blending of various nanoparticles in polymeric matrices has been studied for more than a decade. Most of this effort was focused on improving the mechanical behavior of the nanocomposites and a few such nanocomposites are already in

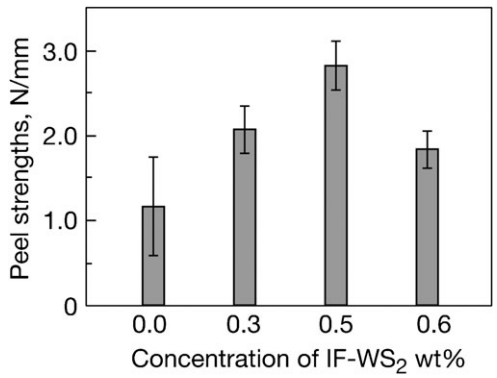

Fig. 11 Peel strength of aluminum joints glued with epoxy resin formulated with different concentrations of IF-WS_2 nanoparticles (courtesy of M. Schneider).[58]

use in the marketplace. More recently, much work was focused on improving the electrical characteristics of polymer matrices. In particular, carbon nanotube nanocomposites have been studied very extensively for variety of applications. Similar studies were extended to IF-WS_2 nanoparticles and more recently INT-WS_2 once they became available in substantial quantities. A series of detailed works on the effect of minute amounts of IF-WS_2 nanoparticles on the thermal stability; crystallinity and the mechanical properties of variety of thermoplastic polymer nanocomposites has appeared.[17,56] It was thus shown[56] that adding a few percent IF-WS_2 nanoparticles to poly(propylene) had a remarkable effect on the thermal stability of the nanocomposite, *i.e.* 60 degrees increase in the initial degradation temperature of this polymer. Furthermore, the nucleation density for crystallization of the polymer matrix was increased by the impregnated IF nanoparticles. Consequently, the storage modulus also increased by 20% and > 30% by blending, respectively, 4 and 8 wt% of the nanoparticles into the polymer matrix. In another study, polyether–ether–ketone (PEEK), an important thermoplastic polymer, was formulated with IF-WS_2 nanoparticles.[57] The nanoparticles were shown to endow enhanced mechanical and tribological behavior to this nanocomposite. In another study, addition of just 0.5 wt% of the nanoparticles to an epoxy resin (D.E.R. 331 with Versamide 140 as curing agent) brought about an almost factor of three enhancement in the peel and shear strength of the contact (see Fig. 11).[58] Clear evidence for the formation of C–O–S bonds between the epoxy resin and the outermost sulfide layer was obtained from IR measurements. The formation of this bond was responsible for crack-bowing and deflection which were clearly observed in the fractured surfaces of the nanocomposite.

IV.c Long-term potential applications

There has been much discussion about the use of nanomaterials including IF/INT to mitigate the anthropogenic effects caused by human activity on the energy supply and its environmental impact. A few publications indicated the catalytic effect of *e.g.* MoS_2 nanotubes on the hydrodesulfurization of oil. The formation of perhydrogenated III–V nanotubes was recently discussed.[59] Other than BN, which exhibits stable (sp^2 hybridized) bonding, all other III–V compounds come as wurzite or zinc-blend (sp^3) structures. Thus for the III–V compounds to form single-wall nanotubes the extra dangling bond which points outwards would have to be passivated. This situation can promote the chemisorption of hydrogen. Such hydrogen-enriched nanomaterials could be favorably considered for hydrogen storage. It was shown[59] that the hydrogen atoms prefer to be on the outer perimeter of the nanotubes for diameters smaller than 1 nm and *vice versa* for nanotubes with larger diameters. These calculations also indicate that nanotubes with the (110) face pointing outwards are preferred over the more polar (111) face.

V. Conclusions

A rich new field of chemistry has been opened by the observation that inorganic compounds with layered structures, like MoS_2 and $NiCl_2$ are unstable in the planar form in the nano-size-range. Generically, 1D inorganic nanotubes (INT) are obtained by folding such nanoparticles in one direction and fullerene-like structures (IF) are formed by folding in two directions. Furthermore, using templated growth, nanotubes of compounds with isotropic lattice (3D), like those from III–V compounds, have been prepared. The synthesis of such nanostructures was found to be a formidable task. Elucidation of the growth mechanism permitted scaling-up of the production of such nanostructures, notably the recent success with WS_2 nanotubes.

The stability of inorganic nanotubes and fullerene-like nanoparticles has been studied in some detail. Experimental work and mostly *ab initio* calculations clearly indicate that such nanostructures are highly strained but nevertheless (meta)stable over a limited (nano)size-range. It has been shown that 3–7 nm nanooctahedra of MoS_2 are the smallest hollow closed polyhedra of this compound, *i.e.* the true inorganic fullerenes.

The study of the chemical and physical behavior of IF and INT is in its early stages. Some interesting observations regarding the mechanical properties of individual INT-WS_2 (MoS_2) and more recently IF-WS_2 were undertaken. Very good agreement between *ab initio* and continuum mechanics calculations on the one hand and experimental data on the other hand, has been obtained suggesting unique failure mechanisms for such nanostructures. In particular, INT-WS_2 were found to be very strong (16 GPa) and flexible (> 10% strain) making them very suitable as strengthening elements in nanocomposites. Indeed, recent publications indicate a great deal of potential by using small amounts of such nanoparticles in interwoven and formulated nanocomposites. IF-WS_2 and IF-MoS_2 were found to be very good solid-state lubricants with numerous potential applications in both lubricating fluids and in self-lubricating coatings. Much more work is needed in order to understand the mechanism of tribological action of such nanoparticles and improve their performance as solid lubricants.

Acknowledgements

We are grateful to Prof. G. Seifert and Dr A. Enayashin (TU Dresden); Drs R. Popovitz, R. Rosentsveig, and A. Albu-Yaron (Weizmann Institute); Drs A. Zak and M. Genut (“NanoMaterials”); Prof. L. Rapoport (Holon Inst. Tech.).

The support of the ERC project *INTIF* 226639; Israel Science Foundation is acknowledged. This work was also supported by the Harold Perlman Foundation and the Irving and Cherna Moskowitz Center for Nano and Bio-Nano imaging. RT is the holder of the Drake Family professorial chair in Nanotechnology and is the director of the Helen and Martin Kimmel Center for Nanoscale Science.

References

1 R. Tenne, L. Margulis, M. Genut and G. Hodes, *Nature*, 1992, **360**, 444.
2 L. Margulis, G. Salitra, R. Tenne and M. Talianker, *Nature*, 1993, **365**, 113.
3 Y. Feldman, E. Wasserman, D. J. Srolovitz and R. Tenne, *Science*, 1995, **267**, 222.
4 N. G. Chopra, J. Luyken, K. Cherry, V. H. Crespi, M. L. Cohen, S. G. Louie and A. Zettl, *Science*, 1995, **269**, 966.
5 R. Kreizman, S.-Y. Hong, J. Sloan, R. Popovitz-Biro, A. Albu-Yaron, G. Tobias, B. Ballesteros, B. G. Davis, M. L. H. Green and R. Tenne, *Angew. Chem., Int. Ed.*, 2009, **48**, 1230.
6 M. Remškar, A. Mrzel, M. Viršek and A. Jesih, *Adv. Mater.*, 2007, **19**, 4276.
7 A. Zak, L. Sallacan-Ecker, A. Margolin, M. Genut and R. Tenne, *Nano*, 2009, **4**, 91.
8 (*a*) D. Golberg, P. M. F. J. Costa, M. Mitome and Y. Bando, *J. Mater. Chem.*, 2009, **19**, 909, Feature Article; (*b*) Y. Sun, J. Hu, Z. Chen, Y. Bando and D. Golberg, *J. Mater. Chem.*, 2009, **19**, 7592, Feature Article.
9 H. J. Fan, U. Goesele and M. Zacharias, *Small*, 2007, **3**, 1660.
10 L.-W. Yin, Y. Bando, Y.-C. Zhu, M.-S. Li, C.-C. Tang and D. Golberg, *Adv. Mater.*, 2005, **17**, 213.
11 M. B. Sadan, L. Houben, A. Enyashin, G. Seifert and R. Tenne, *Proc. Natl. Acad. Sci. U. S. A.*, 2008, **105**, 15643.
12 A. N. Enyashin, S. Gemming and G. Seifert, *Springer Series in Materials Science*, 2007, **93**, 33.
13 I. Kaplan-Ashiri, S. R. Cohen, K. Gartsman, V. Ivanovskaya, T. Heine, G. Seifert, I. Wiesel, H. D. Wagner and R. Tenne, *Proc. Natl. Acad. Sci. U. S. A.*, 2006, **103**, 523.
14 M. N. Tahir, N. Zink, M. Eberhardt, H. A. Therese, U. Kolb, P. Theato and W. Tremel, *Angew. Chem., Int. Ed.*, 2006, **45**, 4809.
15 R. Rosentsveig, R. Tenne, A. Gorodnev, N. Feuerstein, H. Friedman, N. Fleischer, J. Tannous and F. Dassenoy, *Tribol. Lett.*, 2009, **36**, 175.
16 A. Katz, M. Redlich, L. Rapoport, H. D. Wagner and R. Tenne, *Tribol. Lett.*, 2006, **21**, 135.
17 M. Naffakh, C. Marco, M. A. Gomez and I. Jimenez, *J. Phys. Chem. B*, 2008, **112**, 14819.
18 C. Y. Zhi, Y. Bando, W. L. Wang, C. C. Tang, H. Kuwahara and D. Golberg, *J. Nanomater.*, 2008, 642036.
19 C. N. R. Rao and A. Govindaraj, *Adv. Mater.*, 2009, **21**, 4208–4233.
20 R. Rosentsveig, A. Margolin, A. Gorodnev, R. Popovitz-Biro, Y. Feldman, Y. Novema, L. Rapoport, G. Naveh and R. Tenne, *J. Mater. Chem.*, 2009, **19**, 4368.
21 N. Zink, H. A. Therese, J. Pansiot, A. Yella, F. Banhart and W. Tremel, *Chem. Mater.*, 2008, **20**, 65.
22 A. Yella, E. Mugnaioli, M. Panthoefer, H. A. Therese, U. Kolb and W. Tremel, *Angew. Chem., Int. Ed.*, 2009, **48**, 6426.
23 A. N. Enyashin, R. Kreizman and G. Seifert, *J. Phys. Chem. C*, 2009, **113**, 13664–13669.
24 R. Kreizman, *et al.*, to be published.
25 H. J. Fan, U. Gösele and M. Zacharias, *Small*, 2007, **3**, 1660.
26 M. B. Ishai and F. Patolsky, *J. Am. Chem. Soc.*, 2009, **131**, 3679.
27 N. J. Quitoriano, M. Belov, S. Evoy and T. I. Kamins, *Nano Lett.*, 2009, **9**, 1511.
28 J. In, K. Seo, S. Lee, H. Yoon, J. Park, G. Lee and B. Kim, *J. Phys. Chem. C*, 2009, **113**, 12996.
29 J. Hu, Z. Chen, H. Jiang, Y. Sun, Y. Song, H. Chen, H. Chen, D. Golberg, Y. Bando and J. Nid, *J. Mater. Chem.*, in press.
30 G. Chen, C. Xu, X. Song, W. Zhao, Y. Ding and S. Sun, *Inorg. Chem.*, 2008, **47**, 723.
31 L. Gonzalez-Rovira, J. M. Sanchez-Amaya, M. Lopez-Haro, E. del Rio, A. B. Hungria, P. Midgley, J. J. Calvino, S. Bernal and F. J. Botana, *Nano Lett.*, 2009, **9**, 1395.
32 D. Wang, C. Hao, W. Zheng, X. Ma, D. Chu, Q. Peng and Y. Li, *Nano Res.*, 2009, **2**, 130.
33 K. H. Park, J. Choi, H. J. Kim, J. B. Lee and S. U. Son, *Chem. Mater.*, 2007, **19**, 3861.
34 D. B. Seley, M. Nath and B. A. Parkinson, *J. Mater. Chem.*, 2009, **19**, 1532.
35 S. Song, Y. Zhang, Y. Xing, C. Wang, J. Feng, W. Shi, G. Zheng and H. Zhang, *Adv. Funct. Mater.*, 2008, **18**, 2328.
36 G. Jia, K. Liu, Y. Zheng, Y. Song, M. Yang and H. You, *J. Phys. Chem. C*, 2009, **113**, 6050.
37 R. Yan, W. Liang, R. Fan and P. Yang, *Nano Lett.*, 2009, **9**, 3820.
38 A. N. Enyashin, S. Gemming, M. Bar-Sadan, R. Popovitz-Biro, S. Y. Hong, Y. Prior, R. Tenne and G. Seifert, *Angew. Chem., Int. Ed.*, 2007, **46**, 623.
39 M. B. Sadan, L. Houben, S. G. Wolf, A. Enyashin, G. Seifert, R. Tenne and K. Urban, *Nano Lett.*, 2008, **8**, 891.
40 J. M. Gordon, E. A. Katz, D. Feuermann, A. Albu-Yaron, M. Levy and R. Tenne, *J. Mater. Chem.*, 2008, **18**, 458.
41 L. Guimarães, A. N. Enyashin, J. Frenzel, T. Heine, H. A. Duarte and G. Seifert, *ACS Nano*, 2007, **1**, 362.
42 W. Wang, Y. Bando, C. Zhi, W. Fu, E. Wang and D. Golberg, *J. Am. Chem. Soc.*, 2008, **130**, 8144.
43 F. Kopnov, Y. Feldman, R. Popovitz-Biro, A. Vilan, H. Cohen, A. Zak and R. Tenne, *Chem. Mater.*, 2008, **20**, 4099.
44 T. P. Maslennikova, E. N. Korytkova, I. A. Drozdova and V. V. Gusarov, *Russ. J. Appl. Chem.*, 2009, **82**, 352.
45 X. W. Lou, D. Deng, J. Y. Lee, J. Feng and L. A. Archer, *Adv. Mater.*, 2008, **20**, 258.
46 K. Maeda, M. Eguchi, S.-H. Anna Lee, W. J. Youngblood, H. Hata and T. E. Mallouk, *J. Phys. Chem. C*, 2009, **113**, 7962.
47 I. Kaplan-Ashiri, S. R. Cohen, Y. Wang, G. Seifert, H. D. Wagner and R. Tenne, *J. Phys. Chem. C*, 2007, **111**, 8432.
48 M. Virsek, A. Jesih, I. Milosevic, M. Damnjanovic and M. Remskar, *Surf. Sci.*, 2007, **601**, 2868.
49 S. D. Yu, L. X. Chang, H. B. Yang, B. B. Liu, Y. Y. Hou, L. Wang, M. G. Yao, T. Cui and G. T. Zou, *J. Phys.: Condens. Matter*, 2007, **19**, 425228.
50 S. Konduri, S. Mukherjee and S. Nair, *Phys. Rev. B: Condens. Matter Mater. Phys.*, 2006, **74**, 033401.
51 B. Creton, D. Bougeard, K. S. Smirnov, J. Guilment and O. Poncelet, *J. Phys. Chem. C*, 2008, **112**, 10013.
52 H. E. Unalan, Y. ang, Y. Zhang, P. Hiralal, D. Kuo, S. Dalal, T. Utler, S. N. Cha, J. E. Jang, K. Chremmou, G. Lentaris, D. Wei, R. Rosentsveig, K. Suzuki, H. Matsumoto, M. Minagawa, Y. Hayashi, M. Chhowalla, A. Tanioka, W. I. Milne, R. Tenne and G. A. J. Amaratunga, *IEEE Trans. Electron Devices*, 2008, **55**, 2988.
53 C. Shahar, D. Zbaida, L. Rapoportb, H. Cohen, T. Bendikov, J. Tannous, F. Dassenoy and R. Tenne, *Langmuir*, in press.
54 G. R. Samorodnitzky-Naveh, M. Redlich, L. Rapoport, Y. Feldman and R. Tenne, *Nanomedicine*, 2009, vol. 4, issue 8 (ISSN 1743-5889).
55 D. B. Mohan and A. Cavaleiro, *Vacuum*, 2009, **83**, 1257.
56 M. Naffakh, Z. Martin, N. Fanegas, C. Marco, M. A. Gomez, I. Jimenez and J. Polymer Sci, *J. Polym. Sci., Part B: Polym. Phys.*, 2007, **45**, 2309.
57 X. Hou, C. X. Shan and K.-L. Choy, *Surf. Coat. Technol.*, 2008, **202**, 2287.
58 M. Schneider, H. Dodiuk, S. Kenig and R. Tenne, *J. Adhes. Sci. Tech.*, in press.
59 J. T. Tanskanen, M. Linnolahti, A. J. Karttunen and T. A. Pakkanen, *J. Phys. Chem. C*, 2009, **113**, 10065.

